I. Alexeev, U. Quentin, K.-H. Leitz, J. Strauß, M. Baum, F. Stelzle, and M. Schmidt

7 Optical trap assisted sub diffraction limited laser structuring

Abstract: The ability to structure surfaces on a submicron scale is becoming increasingly important for a broad range of technical and biological applications. Such structures can be produced via irradiating micron sized transparent particles placed over a substrate of interest with ultrafast laser pulses. To enhance the structuring flexibility of this method particles can be optically trapped and spatially manipulated relative to the structured surface in order to achieve arbitrary patterns. In this contribution the authors describe the principle of optical trap assisted nanostructuring and present simulated and experimental results demonstrating the potential and limitations of this innovative nanoscale optical material processing technology.

7.1 Introduction

Optical and especially laser based fabrication methods are commonly used to produce structures with characteristic dimensions on a micron and submicron spatial scale. Submicron structuring is often performed using photolithographic methods and although extremely capable (currently achieving spatial feature sizes of 22 nm and targeting 14 nm in the near future [1]) they have wellknown drawbacks of complexity and high cost. Alternatively, nonphotolithographic direct write laser processing [2, 3] can be relatively straightforward, inexpensive, and flexible but the achievable minimum structural feature size of such methods remains to be investigated. As a first approximation the feature size of a direct write technique is assumed to be limited by optical diffraction and determined by the size of the focused laser beam (Fig. 7.1 (a)). In the case of an ideal Gaussian beam the focal spot radius is given by (7.1) [4]

$$r_{\mathrm{fG}} = \frac{\lambda f}{\pi r_{\mathrm{beam}}}, \tag{7.1}$$

where λ is the laser wavelength, f is the focal length of the focusing lens, and r_{beam} is $1/e^2$ radius of the incident beam. The equation inexplicitly assumes that the incident laser beam diameter is small compared to the size of the focusing optics and the diffraction effects from the lens edges are negligible. This is typically not the case when a short focal length microscope objective is used for focusing since its entrance pupil is commonly overfilled by the incident laser beam to utilize the full lens aperture (although overfilling leads to a significant portion of laser beam energy being wasted it, however, permits achievement of smaller focal spots). Overfilling is achieved via spatial magnification of the incident laser beam to a size larger than the lens entrance

aperture and use of the central beam area only effectively reducing the beam intensity variation across the pupil. Hence the incident laser beam can be approximated by a plane wave and the focal radius is calculated using (7.2) which gives a distance from the central maximum to the first intensity zero of the Airy disk in the focal plane [4]

$$r_{\mathrm{fA}} = \frac{0.61\lambda}{\mathrm{NA}}, \tag{7.2}$$

where NA is the numerical aperture of the lens (it should be kept in mind that equations (7.1) and (7.2) define beam radii at different intensity levels and cannot be compared directly). Although equation (7.2) effectively states that a laser beam cannot be focused to a size smaller than half of its wavelength (in air NA $<$ 1), there are a number of methods of circumventing its effect on the achievable minimum structural feature size in the case of laser material processing applications allowing fabrication of structures with characteristic dimensions below the stated value. Some of these approaches are based on the specifics of light-matter interaction processes and take advantage of various material effects to achieve feature sizes below the diffraction limit. The nonlinear (power) dependence of the multiphoton absorption process on electric field intensity allows subfocal confinement of the laser-matter interaction zone. This is exploited for example in the two-photon polymerization technique [5–7] or glass structuring with ultrafast lasers [8]. The threshold-like behavior of ultrafast laser ablation permits removal of material from an area smaller than the laser beam focal spot via careful adjustment of the peak fluence (Fig. 7.1 (b)) [9, 10]. Fabrication of nanostructures has also been attained using near-field techniques incorporating inhomogeneous evanescent waves present at the boundaries to achieve subdiffraction resolution. Here small apertures [11], tips [12], and particles [13] have been used to focus laser beams onto substrates positioned in close proximity to the focusing element (Fig. 7.1 (c)). A combination of near-field and threshold based methods can lead to even smaller structural feature sizes (Fig. 7.1 (d)).

Focusing a laser beam with microscopic dielectric spheres has been extensively investigated both theoretically and experimentally successfully demonstrating its nanostructuring capabilities [14–17]. The approach appears to be particularly efficient for large surface area nanopatterning via deposition of a monolayer of microspheres which acts as an array of microlenses and irradiating them with a large area laser beam [18]. Although such coatings also known as contacting particle lens arrays (CPLA) are of interest for a number of applications [19, 20] variability of the achievable patterns is quite low due to the self-organizing behavior of the colloidal particles which tend to settle into highly periodic hexagonlike shapes. In order to address the issue of CPLA structuring inflexibility while preserving its ability to produce nanoscale structures a sequential patterning method which attempts to combine near-field focusing with optical trapping has been investigated by a number of research groups [21, 22]. Here, a micron size transparent dielectric bead is confined using established principles of optical tweezing and spatially manipulated in 2D or 3D space using

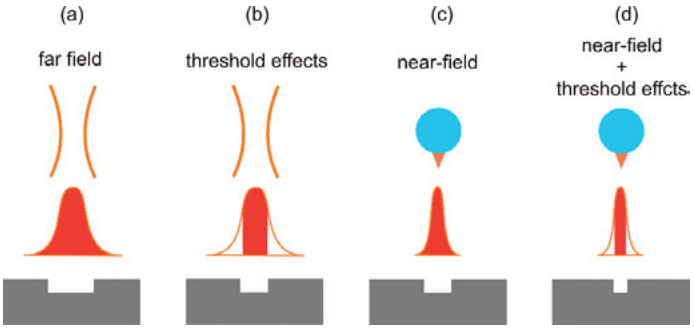

Fig. 7.1: Feature size reduction in laser based structuring: (a) restriction of feature size by diffraction in the far-field; (b) reduction of feature size by utilization of threshold effects; (c) reduction of feature size by utilization of near-field effects; and (d) further reduction of feature size via combination of near-field and threshold effects. Adopted with permission from [42].

either high precision positioning equipment or adaptive optics integrated into the trapping laser beam path. By displacing the bead with respect to the surface of interest and simultaneously irradiating it with an additional structuring laser beam, almost arbitrary surface patterns can be produced with feature sizes below the diffraction limit. In this work the authors present their findings in the field of optical trap assisted laser nanopatterning (OTAN) obtained within the scope of the DFG priority program SPP1327. In the following sections we will present numerical modeling of laser beam focusing with an optically trapped microsphere, experimental investigations of the beadassisted structuring processes, and demonstrate several applications.

7.2 Optical trapping

The key point of the approach investigated is application of optical trapping for precise spatial manipulation of the structuring bead(s). In general, the technique of optical trapping (also known as optical tweezing) is a well-established method which allows noncontact manipulation of micron or submicron sized objects of various origins [23–25]. Optical tweezers are commonly built around a relatively low power continuous wave laser emitting a high quality light beam. The beam is tightly focused with a high numerical aperture microscope objective (typically NA > 1) forming a potential well deep enough to spatially confine a small particle (typically under 10 microns in diameter) [26]. Lens numerical aperture can exceed a value of 1 for immersion objectives since NA $= n \sin\theta$, where n is the index of refraction of the lens working medium. Optical trapping is typically performed in a liquid medium with water being the most common ambient environment. For the relatively large dielectric beads ($d \geq \lambda$) used in this research the trapping mechanism can be understood based on the geometrical optics considerations. In the ray optics model, the trapping force originates from the

light refraction as the laser beam enters and exits the dielectric bead. Except for the on axis ray, the light ray propagation direction changes due to refraction. Since light (or rather photons) has momentum, the deviation in the light direction leads to its momentum change while the bead experiences an equal but opposite momentum change according to the law of conservation. If the sphere is displaced from the center of a symmetrical laser beam focus it will experience a net force turning it back. This net force is due to the light intensity variation across the bead: more intense beams impart a larger momentum change towards the focus than less intense beams which impart a smaller momentum change away from the focus. As a result, if the bead is located on the laser beam axis the lateral forces cancel out due to the symmetry while the scattering force in the longitudinal direction is compensated by the axial gradient force leading to a stable trapping of the particle slightly downstream of the beam waist. While a Gaussian optical trap (formed with a tightly focused Gaussian laser beam) restricts particle movement in all spatial directions other beam types which effectively do not possess an intensity gradient along the longitudinal axis, such as Bessel beams for example, can achieve particle confinement only in the lateral plane [27]. Both 3D and 2D tweezing have been used in OTAN applications [21, 28] but here we concentrate on the former approach only since it permits more defined positioning of the structuring bead although it is also more susceptible to surface irregularities such as tilt and roughness. Depending on the medium used to suspend the focusing bead either oil or water immersion objectives with NA $>$ 1 can be used to form the optical trap. If the medium is aqueous then a water immersion lens would form a trap with almost constant stiffness across various depths [22]. On the other hand if the index of refraction of the ambient medium is high, as for the liquid photopolymer NOA84 (Norland Products) $n_{\mathrm{NOA84}} \approx 1.46$ used for the twophoton polymerization studies described later in the chapter, then switching to an oil immersion lens will be beneficial due to a closer match ($n_{\mathrm{oil}} \approx 1.51$ and n_{NOA84}) of the refractive indices. It should be mentioned that the immersion and trapping media are separated by a thin glass slide and do not mix. For this reason both lens types have been used depending on the process being investigated If a non-aqueous medium is used attention should be paid to its viscosity since the drag forces can exceed the trapping force effectively preventing the bead from being manipulated. High viscosity, for example, restricts the number of photopolymers which can be used in combination with the OTAN technique. Additionally, beads of materials with a relatively low index of refraction, such as silica ($n_{\mathrm{SiO2}} \approx 1.45$) may not be trapped if n_{medium} is noticeably higher than n_{water} due to drastically reduced refraction at the bead surface requiring use of a material with a higher n such as polystyrene ($n_{\mathrm{PS}} \approx 1.58$). Simultaneous trapping of several particles is possible, for example, with holographic optical tweezers [29] or by splitting the trapping beam into multiple arms, allowing parallelization of the OTAN technique [30–32].

7.3 Microsphere focusing in liquid media – numerical simulations

7.3.1 General considerations

In order to understand the capabilities and limitations of the OTAN technique it is important to investigate focusing properties of the microbead used for structuring. Compared to the extensively studied case of dielectric microspheres dispersed on dry surfaces there are several important differences for the technique presented which must be considered. The first and most obvious is that the microparticle is surrounded by an optical medium with a much larger index of refraction than air ($n_{\text{air}} = 1$), strongly affecting the bead's focusing properties.

The second difference is rather technical but should still be carefully analyzed. In the optical tweezers setup the final optical element is a high NA microscope objective which tightly focuses the trapping laser beam. Due to the short working distance of such lenses (less than a few mm) the structuring laser beam has to be launched into the experimental sample through the same microscope objective resulting in its (structuring beam) strong focusing. Although sharing this optical element does not necessarily ensure exact overlap of the bead position and the structuring beam focus, it may be incorrect to treat the (structuring) laser beam as a plane or quasi plane wave as is commonly done. Additionally, a lateral displacement of the pre-focused structuring beam may result in a strong asymmetrical distortion of the bead focus. An apparent alternative solution of using counterpropagating laser beams (for trapping and structuring respectively) will likely result in focusing the structuring beam inside the trapping objective lens and its damage effectively making this approach impractical.

The third difference to be considered is that optical trapping permits a nonzero gap between the microsphere and the substrate to be structured meaning that the longitudinal intensity profile of the particle focus should be taken into consideration too.

In order to investigate these differences and the effects of process parameters a numerical simulation model has been developed using the optical module of the COMSOL Multiphysics software. The model calculates a stationary solution of the 3D wave propagation equation (7.3) while ignoring the temporal behavior of the structuring laser pulse. This simplification is justified since the spatial length of even the shortest pulse used in this work (~ 100 fs or 30 µm) is significantly longer than the typical bead size.

$$\nabla \times \mu_r(\nabla \times \vec{E}) - k_0^2 \left(\varepsilon_r - \frac{j\sigma}{\omega \varepsilon_0} \right) \vec{E} = 0 \tag{7.3}$$

Here, E is the electric field, k is the free space wave number, ω is the wave frequency, ε_0 is the vacuum permittivity ε_r and μ_r are the relative permittivity and permeability respectively, and σ is the electrical conductivity. In the model the relative permittivity ε_r is expressed as $\varepsilon_r(\omega) = \hat{n}^2(\omega)$, with the frequency dependent refractive index taken from published sources [33–37]. For polystyrene and water the refractive indices are taken to be complex, for fused silica glass the index is assumed to be real due to

low absorption for the wavelengths of interest, and for photo polymer NOA84 only the real part of the refractive index is used due to a lack of information about its absorption at 800 nm wavelength. The electrical conductivity σ for each material is taken from the database supplied with COMSOL. In the model the electromagnetic wave is assumed to be linearly polarized in the *x-z* plane with the negative *z* axis being the direction of propagation. Boundary conditions have been defined as "perfect electric conductor" for *y-z* planes and "perfect magnetic conductor" for *x-z* planes. The top and bottom boundaries have been described as "scattering boundary conditions" with the incident electric field being defined as a plane wave or a Gaussian beam respectively. Incident electric field geometrical symmetry in the *x-z* and *y-z* planes is assumed to reduce computational efforts (Fig. 7.2). The process parameters which can be varied in the model are the wavelength of the incident laser beam, bead size and material (refractive index), ambient trapping medium (refractive index), and curvature of the incident laser beam front. The wavelength set investigated was 1064 nm, 800 nm, 532 nm, 400 nm, 355 nm, and 266 nm to match wavelengths of the most common ultrafast lasers. The sizes of the silica (SiO_2) and polystyrene (PS) spheres varied between 0.5 µm and 5 µm in diameter – these bead sizes are readily available. Two trapping media have been considered: water and liquid photopolymer NOA84 (both were used in the experimental part of the program). The structured substrate if mentioned, is always assumed to be a common optical glass such as BK-7 to mimic the experimental arrangements described later. In air the bead and the substrate always contact each other while in the liquid media the simulations are effectively done in two steps – first, the presence of the substrate is ignored and the longitudinal position of the field enhancement peak is determined. Second, the substrate surface is aligned with the plane defined in the previous step and the intensity distribution is recalculated (Fig. 7.2). This two-step approach is adopted to consider the influence of the substrate on bead focusing. Figure 7.2 shows exemplary focal intensity distributions formed by silica and polystyrene spherical beads of 2 µm in diameter in air (a), water (b), and photopolymer NOA84 (c). The incident electric field is a linearly polarized plane wave with an amplitude of $E_x = 1$ V/m and a wavelength of 800 nm. In this chapter we define the intensity as the *z*-component of the Poynting vector $S_z = [\vec{E}\,\vec{H}]_z$, since it has been found to be responsible for structure formation in pulsed laser nanofabrication [38]. In the case of the PS bead immersed in photopolymer NAO84 (Fig. 7.2 (c)) the presence of the substrate is not considered since this setup is of primary interest for 3D additive applications where the particle-substrate separation is likely to be non-constant.

For the dry environment (air) peak intensity enhancement occurs almost immediately underneath the bead permitting the use of contacting particles for surface structuring. The focal spots in the substrate surface plane are slightly asymmetrical for both bead types (SiO_2 and PS) with the orthogonal full width at half maximum (FWHM) diameters given in Tab. 7.1. For comparison the size of a diffraction limited focal spot is also redefined at 50 % intensity drop in the principal maximum of the

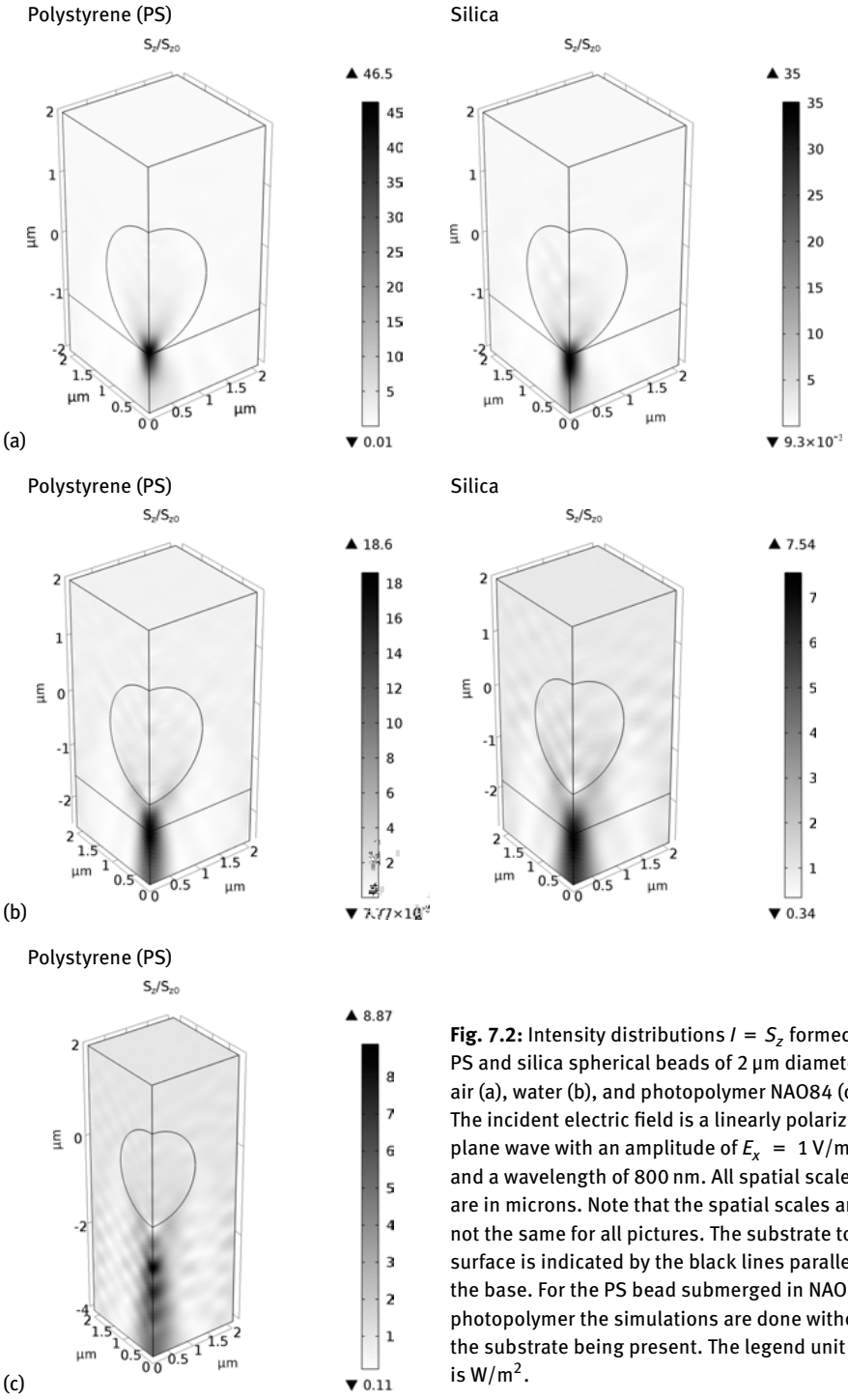

Fig. 7.2: Intensity distributions $I = S_z$ formed by PS and silica spherical beads of 2 μm diameter in air (a), water (b), and photopolymer NAO84 (c). The incident electric field is a linearly polarized plane wave with an amplitude of $E_x = 1$ V/m and a wavelength of 800 nm. All spatial scales are in microns. Note that the spatial scales are not the same for all pictures. The substrate top surface is indicated by the black lines parallel to the base. For the PS bead submerged in NAO84 photopolymer the simulations are done without the substrate being present. The legend unit is W/m^2.

Airy disk resulting in a modified equation (7.2)

$$\mathrm{FWHM}_{\mathrm{fA}} = \frac{0.52\lambda}{\mathrm{NA}}, \tag{7.2'}$$

or $\mathrm{FWHM}_{\mathrm{fA}} \geq 420\,\mathrm{nm/NA}$ at 800 nm wavelength. Based on the simulation results it can be seen that in a dry environment (NA < 1) both bead types focus the incident wave below the diffraction limit promoting contact particle based nanopatterning. Also the results shown in Tab. 7.1 indicate that presence of the substrate should be taken into consideration since it leads to a slight but observable variation of the focal spot size compared to the situation when the particle is levitated in air. A likely reason for such an enlargement is the reduction of the bead focusing power at the contacting area since the index of refraction of the particle is quite close to that of the substrate. The factor of laser intensity enhancement $S_{z\,\mathrm{substrate}}/S_{z0}$ is relatively high for both bead types ensuring that for a broad range of incident intensities only the surface under the particle will be affected.

When the beads are submerged in water (Fig. 7.2 (b)) their focusing power is reduced due to a smaller refractive index difference $n_{\mathrm{bead}} - n_{\mathrm{medium}}$, which becomes apparent in the simulations with the results being less univocal. In the case of the silica bead focusing with the particle becomes equivalent to using a relatively modest 0.75 NA objective, while the PS bead focus still remains smaller than the diffraction limit in air (Tab. 7.1). In this case the threshold effect should be carefully utilized to achieve the desired goal of sub 100 nm minimum feature size. Actually the manifold reduced intensity enhancement factor may favor this approach since a smaller area within the bead focus will exceed the ablation threshold – although care should be taken to avoid structuring with the unfocused beam. Additionally beads made out of optically denser material such as sapphire ($n_{\mathrm{sapphire}} \sim 1.76$) can make the focus tighter with simulations predicting the FWHM diameter to be approximately 340 nm for a 2 µm bead and 800 nm incident beam. Also the longitudinal extent of the focus formed by the sapphire bead is reduced to about 1 µm with the peak intensity formed approximately 150 nm beyond the bead surface. Those focal parameters can make sapphire beads efficient for applications such as biological cell membrane perforation which can be achieved via controllably placing particles with the optical tweezers and irradiating with a structuring laser.

Another important difference compared to the case of dry processing is the existence of a sizable gap between the focusing bead and the substrate (Fig. 7.2 (b)); its formation is consistent with elongation of the bead focal length in water. On the one hand the gap prevents the bead from being damaged or removed after a single pulse irradiation as commonly occurs for the contacting particles permitting reuse of the same microsphere during the structuring process. But on the other hand, the same gap adds an extra degree of complexity namely longitudinal bead position which has to be dealt with. The simulations also show that the influence of the substrate on the beam focusing (when a gap is present) is quite marginal compared to the dry envi-

ronment implying that the experimental procedure can remain the same for different substrate types. Interestingly, the existence of the bead–focus gap allows not only surface patterning but also intramaterial structuring to be performed if the particle is positioned directly on the substrate surface. The proper choice of laser fluence permitted experimental performance of subsurface structuring while preserving the surface integrity, although pulse energies which were too high resulted in both intramaterial modification and surface damage. The latter is likely to occur due to rapid expansion and contraction of glass in the bead focus volume subsequently leading to mechanical microfragmentation.

In the case of the liquid photopolymer NOA84 only PS beads can be used for focusing as silica particles are not capable of light gathering in this environment ($n_{SiO2} < n_{NOA84}$). Here, the PS bead acts as a ball lens with extreme spherical aberrations forming a relatively large focal spot (Fig. 7.2(c)) although the affected zone will be much smaller due to the quadratic intensity dependence of the light-polymer interaction process. Although the bead does not form a very tight focus in the polymer its use may still be preferable to a conventional objective if the lens immersion environment is not optimized for this type of medium.

Tab. 7.1: Simulation results for 2 micron bead focusing of 800 nm wavelength plane wave.

Model configuration	**FWHMx, nm**	**FWHMy, nm**	$S_{z\,\text{substrate}}/S_{z\,0}$	***Bead–Substrate* separation, nm**
SiO2 bead levitated in air	360	330	38	0
PS bead levitated in air	330	390	47	0
SiO2 bead on glass substrate in air	400	340	33	0
PS bead on glass substrate in air	380	320	45	0
SiO2 bead in water with glass substrate	590	580	7.3	900
PS bead in water with glass substrate	420	420	18	500
PS bead in polymer NOA84	460	400	8.7	1000 (bead–$S_{z\,\text{peak}}$ separation)
Sapphire bead in water	330	340	28	150 (bead–$S_{z\,\text{peak}}$ separation)

7.3.2 Variation of structuring wavelength and bead size

The other two process parameters which will strongly influence the structuring process are laser wavelength and bead size (the interaction process itself is not considered in the model) [12] Although they can both assume only discrete values they vary in relatively broad ranges allowing their use in process optimization/control. Figure 7.3 shows the variation of the focal spot FWHM diameter (a) and the enhancement factor (b) beneath a bead submerged in water as a function of its size for both SiO_2 and PS particle types at the laser wavelength of 800 nm. The diameters are measured in the planes of highest enhancement.

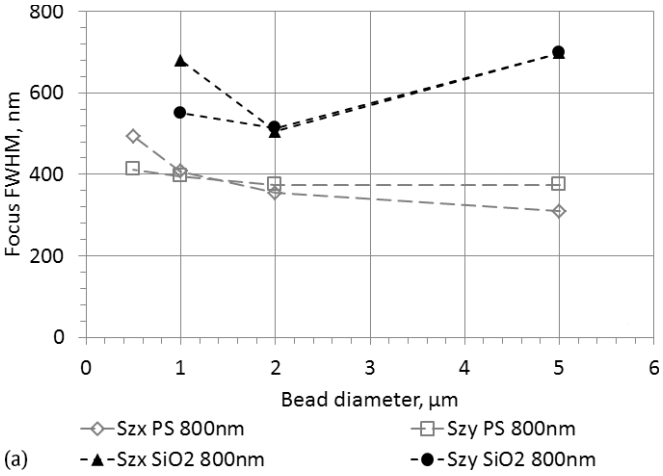

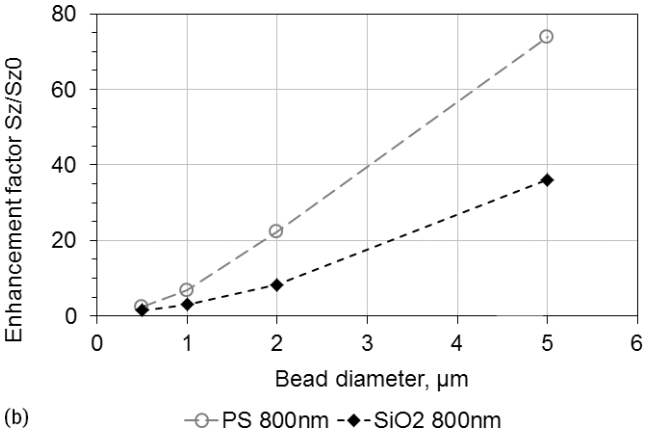

Fig. 7.3: Focus FWHM diameter (a) and enhancement factor (b) beneath a microsphere particle submerged in water vs. particle size (wavelength $\lambda = 800$ nm). The focal diameters are determined in the planes of highest enhancement. The connecting lines are a visual aid only.

As expected, the use of PS particles appears preferable since they always form a smaller focus compared to fused silica. A larger PS bead collects more light to a tighter spot resulting in a higher enhancement factor, but interestingly, it also makes the use of threshold effect more challenging so the size of 2 microns appears to be a good compromise from practical considerations. Figure 7.4 shows the dependence of the focal FWHM diameter on the irradiating laser wavelength. As expected the focal spot gets bigger as the wavelength increases but the focus enlargement is actually more dramatic as linear λ dependence due to the dispersion effect and the corresponding reduction of the refractive indices difference ($n_{\text{bead}} - n_{\text{medium}}$) at longer wavelengths This can be clearly seen as the focal spot size effectively doubles when the wavelength changes from 800 to 1064 nm. Use of short (in the UV region) wavelengths becomes preferable to achieve the targeted feature size of 100 nm and below.

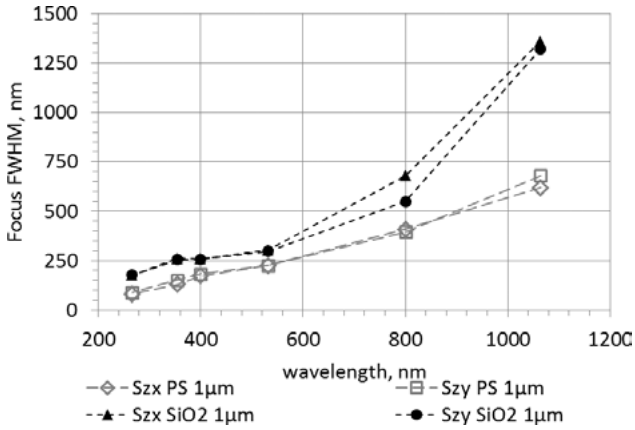

Fig. 7.4: Focus FWHM diameter vs. laser wavelength (particle size $d = 1$ µm), the ambient medium is water. The connecting lines are a visual aid only.

7.3.3 Bead irradiation with a non-plane wave

In general, the structuring laser beam shall not be treated as an infinite plane wave if its focus is located in the proximity of the particle but this scenario can happen since both trapping and structuring beams are focused with the same objective lens (see "Experimental procedure" for more details). To qualitatively illustrate the effect of non-plane wave bead focusing Fig. 7.5 shows an extreme case when the structuring laser beam focal plane is situated on top of a polystyrene bead (of 2 micron diameter) submerged in water. The laser beam focal spot is taken to be 1.5 micron in diameter ($1/e^2$), which is a realistic estimation for the experimental setup described later in the chapter. Since the structuring beam focus is smaller than the particle itself the bead effective NA is decreased leading to weakening of its focusing power and poten-

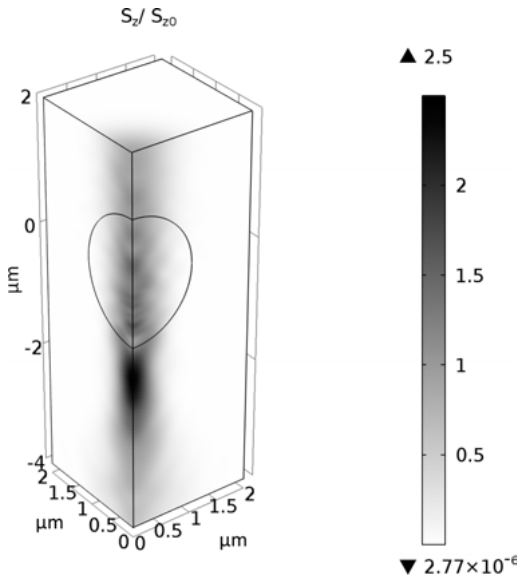

Fig. 7.5: Focusing of a Gaussian beam with $1/e^2$ diameter of 1.5 μm by a 2 μm PS bead in water. The beam focal plane overlaps the top of the bead.

tially defeating the purpose of using the microbead for sub-diffraction focusing. In the example given, the focal FWHM diameters are 540 nm and 580 nm for the x and y direction respectively with the maximum enhancement factor being below 3.

To avoid this scenario the particle should remain irradiated with a fairly uniform laser beam which can be attained by displacing the structuring beam focus downstream. In practice such decoupling of the trapping and structuring beam focal planes is achieved by adjusting the divergence of those beams although the resulting separation may remain fairly small in absolute terms of the order of tens of microns. Nevertheless it is significantly longer than the corresponding Rayleigh range of the structuring beam which is ~ 5 μm, ensuring relatively uniform irradiation of the bead and complete use of its aperture. The structuring beam must be focused beyond the bead; otherwise the particle collimates the beam rather than focuses it. Care should be taken here, however, to avoid surface/volume patterning with the structuring laser beam focus instead of the bead's.

7.4 Experimental procedure

The experimental investigation of the OTAN capabilities was performed using the apparatus described below. While the hardware setup remained pretty much the same for almost all experiments different test samples and process parameters were applied. A typical sample consists of a glass coverslip and an uncoated or polyimide coated soda lime glass slide (to be structured) which seal a volume of aqueous or photopolymer solution of microspheres of constant size and type (a test sample is

schematically shown in Fig. 7.6). Different samples must be used if a variation of partial size or material is desired. The sealed volume is approximately 5 mm × 5 mm × 90 µm with typical bead concentration of $1.7 \cdot 10^5$ particles/ml. This concentration is high enough to ensure the presence of several particles in the field of view of the process monitoring imaging system and sufficiently low to avoid the trapping of multiple beads in the tweezing laser beam focus at the same time The schematic of the OTAN setup is depicted in Fig. 7.6 and can be effectively split into three subsystems. The first subsystem (green) is the trapping arm which consists of either a frequency doubled cw Nd:YAG laser with a wavelength of 532 nm focused through a water immersion objective with NA of 1.2 (used for aqueous bead solutions) or a 1064 nm Nd:YAG laser focused by a 1.25 NA oil immersion objective (used for experiments with the photopolymer). The structuring arm (purple) can employ either an 800 nm/400 nm laser beam from a Ti:Sapphire femtosecond laser (100 fs pulse duration) or a 532 nm beam from a 10 ps high repetition rate Nd:YVO_4 laser. Magnifying telescopes are introduced in both subsystems to control size and divergence of the beams with the latter being necessary to introduce proper separation of the trapping and structuring beam foci. The third subsystem (light orange) is used for imaging of the trapped bead and monitoring of its displacement. The resolution of this subsystem is not sufficient for detailed real time examination of the structures produced; that has to be done later using optical and electron microscopes. For structuring the test sample mounted on a high precision 3D linear translation stage is displaced with respect to the stationary trapping and structuring beams.

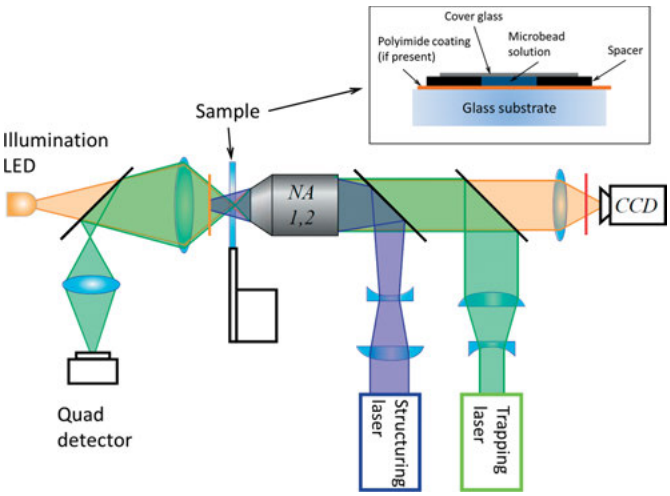

Fig. 7.6: Experimental setup of OTAN. Green path – optical trapping subsystem incorporating either 532 nm or 1064 nm cw laser; purple path – structuring arm which can employ either 800 nm 100 fs, 400 nm 100 fs, or 532 nm 10 ps laser pulses; light orange path – imaging subsystem used for structuring process visualization A typical test sample is schematically shown in the insert.

As discussed earlier in order to perform surface structuring using the OTAN approach the bead must be properly spaced with the sample surface and a correct gap must be maintained during the patterning process. Although the bead longitudinal position can be optimized by performing surface structuring at different particle-substrate separations, effectively using the trial and error approach a more accurate method of axial beam positioning is based on correlating the size of the imaged diffraction pattern of a reference particle with its longitudinal position. As the particle is moved in the axial direction, its diffraction pattern changes and the apparent diameter increases the further it is displaced away from the object plane of the imaging system (Fig. 7.7). Since the change in diameter varies linearly with the distance, this effect can be used to determine the particle position assuming proper calibration coefficients have been established: Gap = Linear Function(Bead Image Size). Such coefficients can be determined based on quantization of a sequence of bead images taken at different particle displacements away from the imaging plane. Quantization is done using multistep image processing analysis which includes denoising, intensity gradient determination, and wavelet thresholding with the sizes of the resulting particle binary images being easily extractable [39]. In practice such surface positioning is done not with a bead that will be used for structuring later on (its position and appearance remain constant in the imaging setup) but with a particle attached to the surface of interest. Such a bead(s) appears to always be present in every sample.

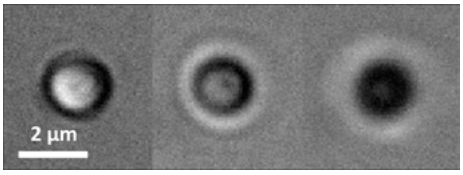

Fig. 7.7: Different axial particle position relative to the object plane leads to different diffraction patterns Adopted with permission from [39].

7.5 Nanostructuring results

7.5.1 Surface nanopatterning

The initial surface nanopatterning was performed on polyimide coated glass substrates using an SiO_2 particle of 2 µm diameter irradiated with 532 nm wavelength 10 ps laser pulses (Fig. 7.8). The pulse fluence (F = 8 mJ/cm^2), feed rate (5 µm/s), and pulse repetition rate (500 Hz) were adjusted to stably produce welldefined structures. In general the laser pulse rate represents a tradeoff between structuring speed and process stability. At high pulse frequencies the structuring bead cannot resettle at the equilibrium position after being displaced by the ablation process thus the pulse frequency is typically kept below 2 kHz to ensure process stability.

The image presented clearly demonstrates the feasibility of surface nanostructuring using optical microbeads trapped with Gaussian tweezers although the achieved

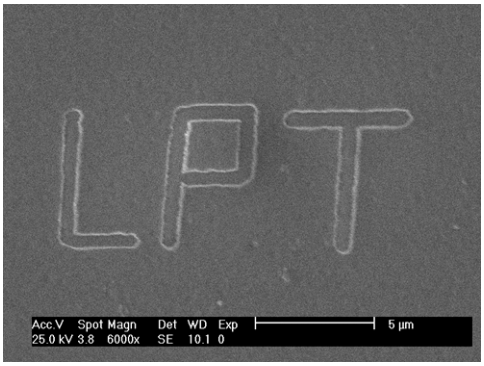

Fig. 7.8: SEM microphotograph of nanostructures on polyimide (EPO-Tek P1011). Process parameters: 2 µm SiO2 microsphere irradiated with $\lambda = 532$ nm, $\tau = 10$ ps, pulse frequency $f = 500$ Hz and fluence $F = 8\,\mathrm{mJ/cm^2}$ laser beam. Image adopted with permission from [28].

characteristic dimensions of the pattern appear to be relatively large – approximately 500 nm line width and 150 nm depth wise. Simulations performed for a matching microsphere irradiated with a 532 nm plane wave predict the bead focal size to be 460 nm FWHM pointing out that surface structuring was performed by the entire focus without using the thresholding effect. Use of 400 nm 100 fs laser pulses and 1 micron beads made it possible to achieve narrower structures (approximately 200 nm wide). It should be pointed out that further reduction of the line width can be limited not only by the size of the bead focus and laser fluence (threshold effect), but also by jitter of the structuring particle around its equilibrium position. Since any nonpoint line-like structure is produced by overlapping multiple shots its characteristic width will be broadened on the level of the average bead position deviation from its mean value: Line Broadening $\sim 2\sigma_{\text{Bead Deviation}}$. Such deviations depend on the properties of the optical trap and have been shown to vary between 30 and 100 nm under typical experimental conditions making line broadening an important limiting factor for structuring processes [39]. This variation can be reduced by the use of stiffer traps (care should be taken not to damage the bead with the trapping beam) and lowering the pulse repetition frequency (unfortunately the latter will also reduce the structuring speed) but ultimately it will still be limited by pointing stability of the trapping laser and Brownian motion (the latter is on the level of 5 nm). In this case single shot point-like surface structuring can provide more accurate information on the potentially achievable minimum feature size. In these experiments PS particles irradiated with 800 nm laser pulses of different energies were used to make dot-like structures on different test substrates (soda lime glass, fused silica glass, and polyimide coated glass) with the results being presented in Fig. 7.9. The laser pulse energy appears to be the most important "tuning knob" for the structure size utilizing the threshold effect. The smallest feature size achieved remains fairly similar for different particle sizes and substrate materials and appears to be of the order of 200 nm. Further feature size reduction is achievable by shortening the structuring wavelength to 400 nm. This has enabled production of point pattern on polyimide coated substrate with a diameter of 80 nm [40].

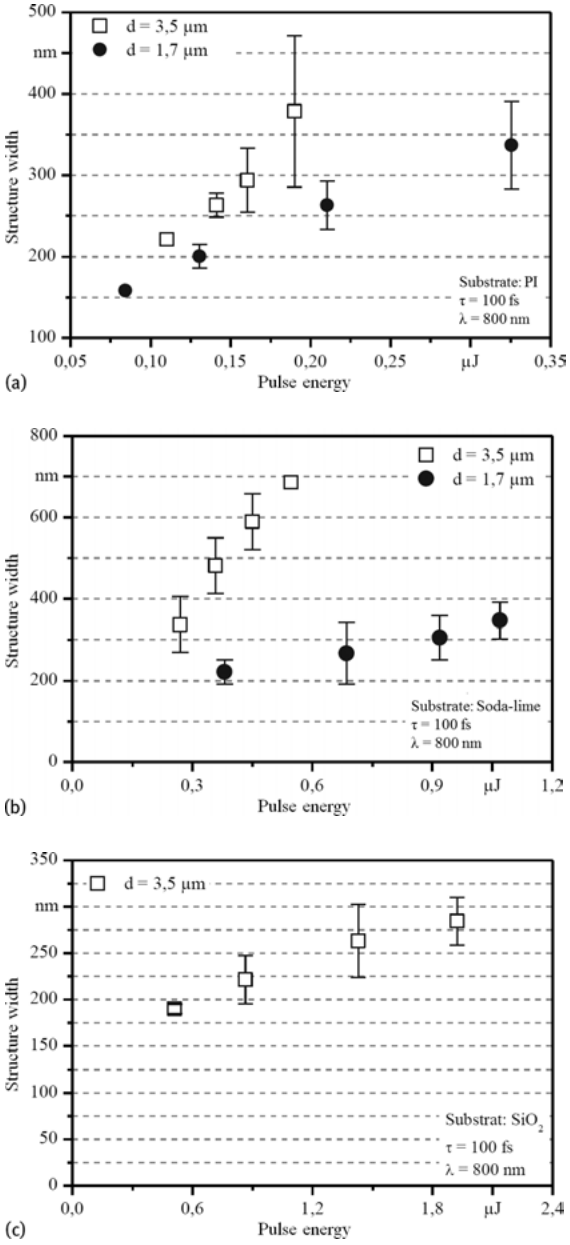

Fig. 7.9: Variation of dot-like structure size on polyimide coating (a), soda lime glass (b), fused silica glass (c) for different laser pulse energies. The laser wavelength is 800 nm and the pulse duration 100 fs. The focusing polystyrene particle sizes are 1.7 µm and 3.5 µm in diameter except for the fused silica substrate; here only 3.5 µm beads have been used.

7.5.2 Multiphoton polymerization

Besides surface and subsurface patterning applications the OTAN technique can be used to create structures via multiphoton material processing. Multiphoton polymerization is based on simultaneous absorption of two or more photons with the total energy sufficient to initiate a photo-polymerization reaction. Since the probability of simultaneous absorption of several photons is a nonlinear function of light intensity polymerization occurs only within the laser beam focus. NOA84 liquid photopolymer is effectively transparent for 800 nm wavelength since its absorption starts below $\lambda = 450$ nm but light intensity can be sufficiently enhanced in the bead focus (Fig. 7.2 (c)) to cause the nonlinear effect. PS particles can be successfully trapped and displaced in NOA84 polymer using the setup described above. When the trapped bead is irradiated with ultrafast laser pulses (100 fs) at fluence levels 5–20 mJ/cm^2 then tracks of polymerized voxels (volumetric pixel) are created on a glass substrate surface. The size of the structures generated is strongly influenced by the process parameters primarily the incident laser fluence with the smallest achieved size being 83 ± 11 nm in diameter (Fig. 7.10) [41].

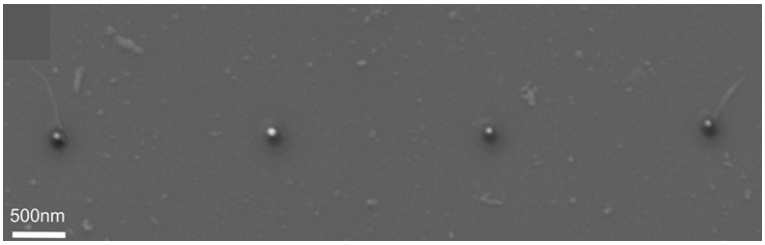

Fig. 7.10: Line of voxel generated by irradiating a 3.5 µm polystyrene microbead in NOA84 photopolymer. Average voxel diameter is 83 ± 11 nm. Image adopted with permission from [41].

7.6 Conclusion

The research conducted has demonstrated the feasibility of using optical trap assisted nanopatterning for surface and subsurface laser structuring. The achievable patterns have flexible geometries with the minimum structural feature size being determined by a number of process parameters. In order to achieve the targeted feature size of 100 nm careful combination of short laser wavelengths with threshold-like ultrafast laser ablation must be utilized simultaneously since the bead focus on its own appears to be larger than the targeted value. Although fabrication of sub 100 nm dot-like structures has been successfully demonstrated the minimal feature size of more complex line-like structures tends to be noticeably larger, at around 200 nm. This increase in feature size can be attributed to the jitter of the structuring bead around the equilib-

rium position due to Brownian motion and the pointing stability of the trapping laser in combination with shot-to-shot energy variation of the structuring laser pulses.

Accurate use of the thresholding effect is a complex task since not only the pulse energy but also the beam focal position must be maintained with a very high degree of accuracy to ensure the same laser intensity during the structuring process. The OTAN technique can provide an advantage for intensity threshold based processing since the position of the bead focus with respect to the particle remains constant while the positioning of the sphere itself can be a simpler task owing to its ease of visualization and tracking. Another exemplary application of the OTAN technique can be for two-photon polymerization since the bead focus should remain constant at different immersion depths compared to conventional microscope objectives which are not designed for such an ambient medium (photopolymer).

References

[1] Bohr M, Mistry K. Intel's revolutionary 22 nm transistor technology. Intel website 2011.
[2] Arnold CB, Piqué A. Laser direct-write processing. MRS bulletin 2007; 32: 9–15.
[3] Gattass RR, Mazur E. Femtosecond laser micromachining in transparent materials. Nature Photon 2008; 2: 219–25.
[4] Saleh BEA, Teich MC. Fundamentals of photonics: John Wiley and Sons, New York, 1991.
[5] Kawata S, Sun H, Tanaka T, Takada K. Finer features for functional microdevices. Nature 2001; 412: 697–8.
[6] Li L, Fourkas JT. Multiphoton polymerization. Materials Today 2007; 10: 30–37.
[7] LaFratta CN, Fourkas JT, Baldacchini T, Farrer RA. Multiphoton Fabrication. Angew. Chem. Int. Ed. 2007; 46: 6238–6258.
[8] Bhuyan MK, Courvoisier F, Lacourt PA, et al. High aspect ratio nanochannel machining using single shot femtosecond Bessel beams. Applied Physics Letters 2010; 97: 081102–081102-3.
[9] Pronko PP, Dutta SK, Squier J, Rudd JV, Du D, Mourou G. Machining of sub-micron holes using a femtosecond laser at 800 nm. Optics communications 1995; 114: 106–110.
[10] Korte F, Serbin J, Koch J, et al. Towards nanostructuring with femtosecond laser pulses. Applied Physics A 2003; 77: 229–235.
[11] Hecht B, Sick B, Wild UP, et al. Scanning near-field optical microscopy with aperture probes: Fundamentals and applications. J. Chem. Phys. 2000; 112: 7761.
[12] Dickmann K, Jersch J, Demming F. Focusing of Laser Radiation in the Near-field of a Tip (FOLANT) for Applications in Nanostructuring. Surface and interface analysis 1997; 25: 500–504.
[13] Huang SM, Hong MH, Lukiyanchuk B, Chong TC. Nanostructures fabricated on metal surfaces assisted by laser with optical near-field effects. Applied Physics A 2003; 77: 293–296.
[14] Luk'yanchuk BS, Arnold N, Huang SM, Wang ZB, Hong MH. Three-dimensional effects in dry laser cleaning. Applied Physics A 2003; 77: 209–215.
[15] Devilez A, Bonod N, Wenger J, et al. Three-dimensional subwavelength confinement of light with dielectric microspheres. Opt. Express 2009; 17: 2089.
[16] Zhou Y, Hong MH, Fuh JY, et al. Direct femtosecond laser nanopatterning of glass substrate by particle-assisted near-field enhancement. Applied Physics Letters 2006; 88: 23110.

[17] Huang SM, Sun Z, Luk'yanchuk BS, Hong MH, Shi LP. Nanobump arrays fabricated by laser irradiation of polystyrene particle layers on silicon. Appl. Phys. Lett. 2005; 86: 161911.
[18] Guo W, Wang ZB, Li L, Whitehead DJ, Luk'yanchuk BS, Liu Z. Near-field laser parallel nanofabrication of arbitrary-shaped patterns. Appl. Phys. Lett. 2007; 90: 243101.
[19] Barnes WL, Dereux A, Ebbesen TW. Surface plasmon subwavelength optics. Nature 2003; 424: 824–830.
[20] Liu K, Cao M, Fujishima A, Jiang L. Bio-Inspired Titanium Dioxide Materials with Special Wettability and Their Applications. Chemical reviews 2014.
[21] McLeod E, Arnold CB. Subwavelength direct-write nanopatterning using optically trapped microspheres. Nat Nanotechnol 2008; 3: 413–417.
[22] Quentin U, Leitz K, Deichmann L, Alexeev I, Schmidt M. Optical trap assisted laser nanostructuring in the near-field of microparticles. J. Laser Appl. 2012; 24: 42003.
[23] Ashkin A, Dziedzic JM, Yamane T. Optical trapping and manipulation of single cells using infrared laser beams. Nature 1987; 330: 769–771.
[24] Svoboda K, Block SM. Optical trapping of metallic Rayleigh particles. Opt. Lett. 1994; 19: 930.
[25] Ashkin A, Dziedzic JM, Bjorkholm JE, Chu S. Observation of a single-beam gradient force optical trap for dielectric particles. Opt. Lett. 1986; 11: 288.
[26] Neuman KC, Block SM. Optical trapping. Review of scientific instruments 2004; 75: 2787–809.
[27] Arlt J, Garces-Chavez V, Sibbett W, Dholakia K. Optical micromanipulation using a Bessel light beam. Optics communications 2001; 197: 239–245.
[28] Quentin U, Leitz K, Alexeev I, Schmidt M. Application of Gaussian optical tweezers for ultrafast laser assisted direct-write nanostructuring. Journal of Laser Micro/Nanoengineering 2012: 7
[29] Curtis JE, Koss BA, Grier DG. Dynamic holographic optical tweezers. Optics communications 2002; 207: 169–175.
[30] McLeod E, Arnold CB. Array-based optical nanolithography using optically trapped microlenses. Opt. Express 2009; 17: 3640.
[31] Tsai Y, Fardel R, Arnold CB. Nanopatterning on rough surfaces using optically trapped microspheres. Appl. Phys. Lett. 2011; 98: 233110.
[32] Tsai Y, Leitz K, Fardel R, Otto A, Schmidt M, Arnold CB. Parallel optical trap assisted nanopatterning on rough surfaces. Nanotechnology 2012; 23: 165304.
[33] Thormählen I, Straub J, Grigull U. Refractive index of water and its dependence on wavelength, temperature, and density. J. Phys. Chem. Ref. Data 1985; 14: 933.
[34] Hale GM, Querry MA. Optical constants of water in the 200-nm to 200-µm wavelength region. Appl. Opt. 1973; 12: 555.
[35] French RH, Winey KI, Yang MK, Qiu W. Optical properties and van der Waals-London dispersion interactions of polystyrene determined by vacuum ultraviolet spectroscopy and spectroscopic ellipsometry. Australian Journal of Chemistry 2007; 60: 251.
[36] Ma X, Lu JQ, Brock RS, Jacobs KM, Yang P. Determination of complex refractive index of polystyrene microspheres from 370 to 1610 nm. Phys. Med. Biol. 2003; 48: 4165.
[37] RefractiveIndex.info (http://refractiveindex.info/). Norland Optical Adhesive 84 (http://www.norlandprod.com/adhesives/NOA%2084.html).
[38] Wang ZB, Joseph N, Li L, Luk'Yanchuk BS. A review of optical near-fields in particle/tip-assisted laser nanofabrication. Proceedings of the Institution of Mechanical Engineers, Part C: Journal of Mechanical Engineering Science 2010; 224: 1113–1127.
[39] Quentin U, Leitz K, Paulus J, Alexeev I, Schmidt M. Positioning Accuracy in Optical Trap Assisted Nanostructuring. Journal of Laser Micro/Nanoengineering 2013; 8.
[40] Quentin U, Berg B, Alexeev I, Schmidt M Optical Trap Assisted Nanostructuring of Glasses and Polymers, Proceedings of LAMP2013 – the 6th International symposium on Laser Advanced Material Processing 2013.

[41] Leitz K, Tsai Y, Flad F, et al. Multiphoton polymerization using optical trap assisted nano-patterning. Appl. Phys. Lett. 2013; 102: 243108.
[42] Leitz K, Quentin U, Alexeev I, Schmidt M. Process investigations of optical trap assisted direct-write microsphere near-field nanostructuring. CIRP Annals-Manufacturing Technology 2012; 61: 207–210.